FUNDAMENTAL UNDERSTANDING AND PREDICTION OF ROTOR VIBRATORY LOADS IN HIGH-SPEED FORWARD FLIGHT

Jayanarayanan Sitaraman **Anubhav Datta** **James D. Baeder** **Inderjit Chopra**

Graduate Research Assistants — Associate Professor — Alfred Gessow Professor

jaina@eng.umd.edu datta@eng.umd.edu baeder@eng.umd.edu chopra@eng.umd.edu

Alfred Gessow Rotorcraft Center
Department of Aerospace Engineering
University of Maryland, College Park, MD 20742

ABSTRACT

This paper reviews the ongoing work at the University of Maryland to identify the fundamental physics of rotor vibrations in high speed flight. Specifically, this work is an attempt to isolate the physics of rotor aerodynamics and structural dynamics from the complex aeroelastic problem, validate and improve them separately and put them back together. Measured lift, chord force, pitching moment and damper force from the UH-60A Airloads Program are used to predict and validate the rotor structural model. Once validated, the blade deformations are prescribed in the aerodynamic models to calculate airloads. The airflow model is refined from a table look up based unsteady lifting-line model to a 3-dimensional Navier-Stokes CFD model. The 3-dimensional CFD model captures the vibratory lift and pitching moments accurately both in magnitude and phase. The CFD model is then used to investigate the physics of the flow field and identify the limitations of the lifting-line model. Finally, the CFD model is loosely coupled with the structural model to obtain an improved aeroelastic solution from first principles.

INTRODUCTION

The objective of this paper is to improve the fundamental understanding and prediction of rotor vibratory loads by separating the physics of aerodynamics and structural dynamics. The focus is on high-speed flight (155 kts, $\mu = 0.368$). The state-of-the-art in helicopter vibration prediction in high-speed flight is far from satisfactory [1] (Fig 1) even though both vibratory airloads and structural response show consistent patterns for a large number of helicopters [2], [3]. Prediction accuracy of vibratory blade loads is less than 50%. Lift and pitching moment measurements from the UH-60A Airloads Program [4] opens the opportunity for tracing back the sources of prediction deficiencies to discrepancies in the airload calculation.

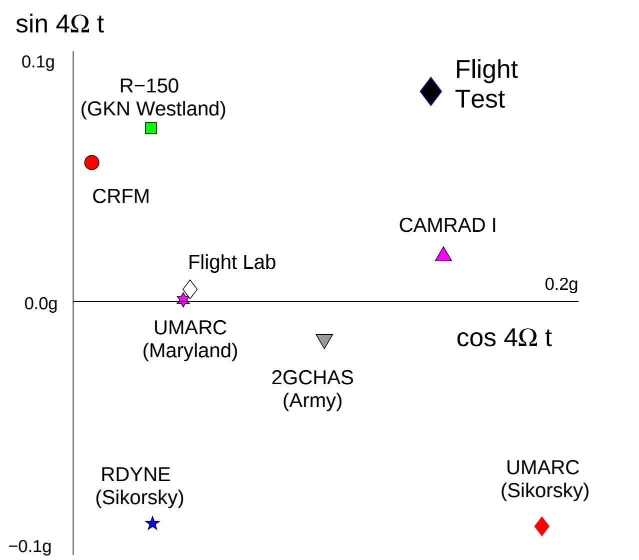

Figure 1: **Vibratory hub load predictions from eight aeroelastic codes compared with Lynx data, Cockpit starboard location, 158 knots (1996 AHS Dynamics Workshop)**

Bousman in 1999 [5] identified two key discrepancies: first, phase prediction of advancing blade lift in high-speed flight and second, prediction of section pitching moments. Figure 2 shows the lift and pitching moment predictions from a baseline comprehensive analysis UMARC (University of Maryland Advanced Rotorcraft Code) using a detailed swept tip model [6], an airfoil table look-up based lifting-line model, free wake (Bagai-Leishman [7]) and a 2-dimensional (2D) subsonic unsteady flow model (Leishman-Beddoes, [8, 9]). UMARC

Presented at the 29th European Rotorcraft Forum, Friedrichshafen, Germany, Sep 16-18, 2003.

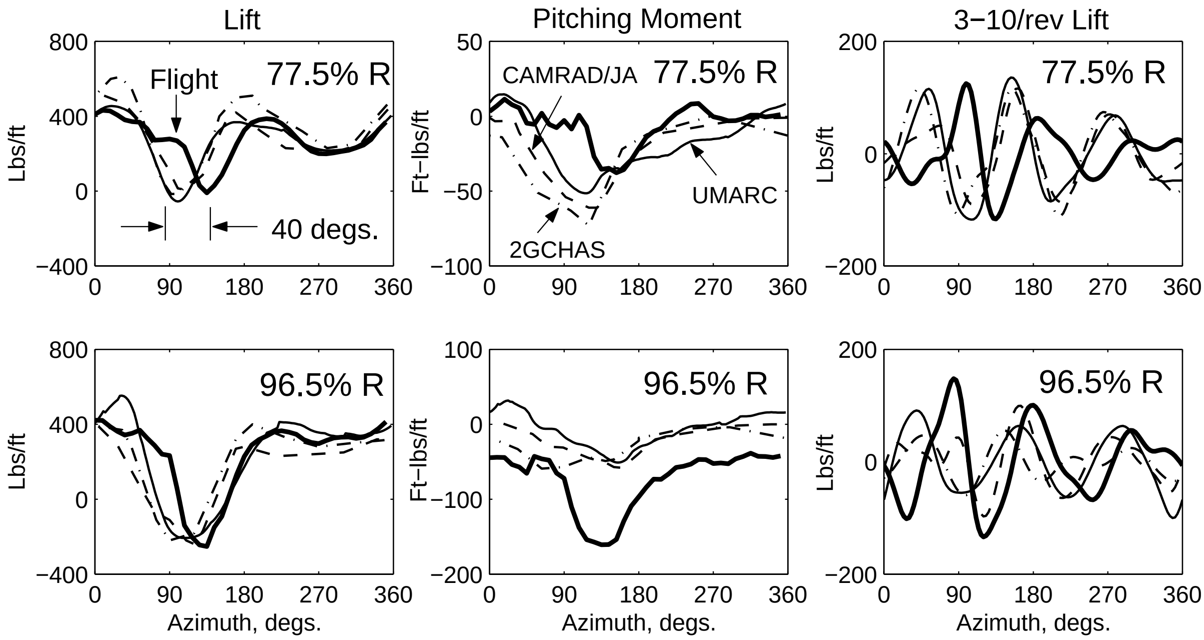

Figure 2: **State-of-the-art predictions of lift and pitching moment for the UH-60A Black Hawk in high-speed level flight; μ = 0.368, C_w/σ = 0.0783**

predictions show similar results compared to other state-of-the-art comprehensive analyses CAMRAD/JA and 2GCHAS (1994, [12]). At 77.5% radius, the error in the lift phase occurs together with a premature drop in predicted pitching moment. However, at 92% radius, prediction shows a delay in pitching moment drop with no corresponding delay in lift phase.

The section pitching moments determine elastic torsion which directly affects the blade lift as a contributing component of the angle of attack. Reference [10] showed that the lift phase problem stems from inaccurate prediction of vibratory lift (3/rev and higher harmonics), the dominant source of which is an up-down excitation on the advancing blade. Figure 2 shows the inaccurate prediction of vibratory lift from all comprehensive analyses. Reference [10] further showed that the lift on the advancing blade is dominated by elastic torsion deformation. Elastic torsion is governed by predicted pitching moments. Pitching moment predictions are not reliable. All codes over-predict the moments inboard and under-predict near the tip. Thus, accurate prediction of lift and pitching moment are related to each other and with the accuracy of structural response calculation.

The intent of this paper is to decouple these two effects. Aerodynamic and structural response data used in the present study are obtained from the UH-60A (Army/NASA) Airloads Program. UMARC is used as the structural analysis platform. The Transonic Unsteady Reynolds-averaged Navier Stokes (TURNS) research code is used for CFD calculations [13].

METHODOLOGY

In the first step, measured airloads, damper force and rotor control angles from the UH-60A Airloads Program are used to calculate structural response of an isolated rotor. A similar study was carried out in reference [14] using flight test and wind tunnel airloads of a CH-34 rotor. The equations governing flap and lag degrees of freedom were coupled by the local pitch angle. Torsion degree of freedom was uncoupled from flap and lag. In the present study, a fully coupled set of equations are used, as derived in references [15, 16]. The equations are coupled via sectional center of gravity offsets, blade sweep, and local pitch angle. Another similar investigation was later carried out in Reference [17] for the UH-60A but the airloads used were that of a model scale rotor.

In the second step, blade deformations calculated above are used to predict airloads. There are no measured blade deformations and hence deformations calculated using measured airloads are used. Reference [18] carried out a similar study on a model scale UH-60A rotor. The flap and lag deformations were obtained similarly but torsion deformation was derived from strain gage data using a modal method. The focus of reference [18] was on unsteady aerodynamics and wake methodologies. In the present study, the focus is on 3-dimensional (3-D) flow and compressibility effects.

In the third step, 3-D CFD calculations are studied systematically to understand the role of blade motions, transonics, forward flight speed and 3-D aerodynamic effects in the generation of vibratory airloads.

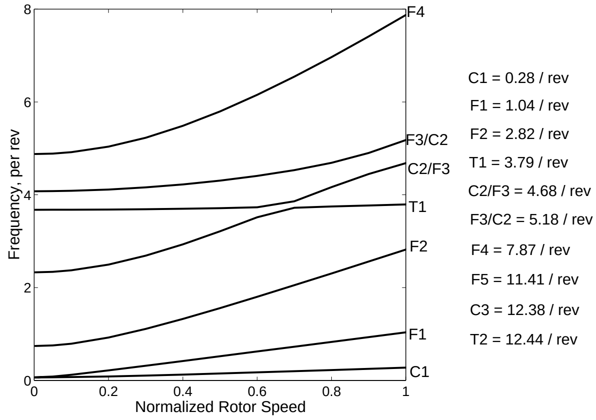

Figure 3: **UH-60A rotor blade frequencies *in vacuo*; F:Flap, L:Lag, T:Torsion**

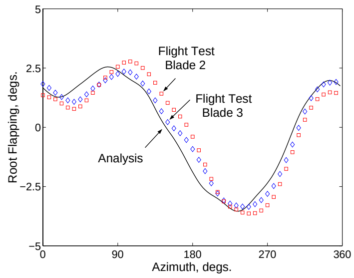

Figure 4: **Calculated root flap angle using measured airloads; $C_W/\sigma = 0.0783$, high speed $\mu = 0.368$**

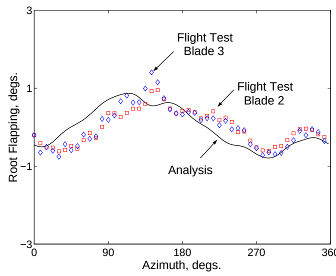

Figure 5: **Calculated root lag angle using measured airloads; $C_W/\sigma = 0.0783$, high speed $\mu = 0.368$**

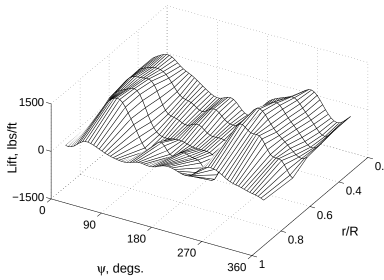

(a) Measured flap bending moment (1-10/rev)

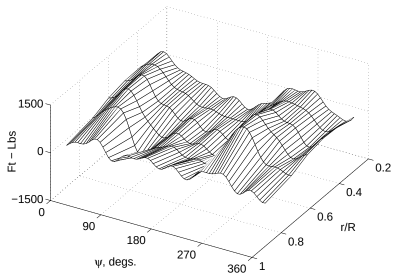

(b) Predicted flap bending moment (1-10/rev)

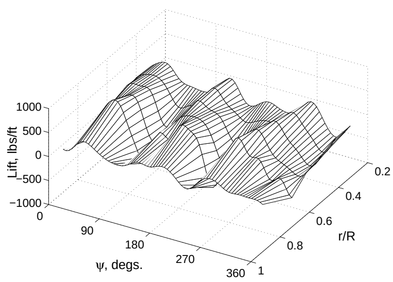

(c) Measured vibratory flap bending moment (3-10/rev)

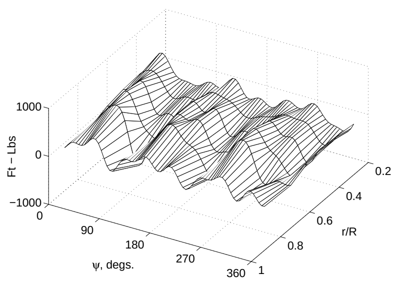

(d) Predicted vibratory flap bending moment (3-10/rev)

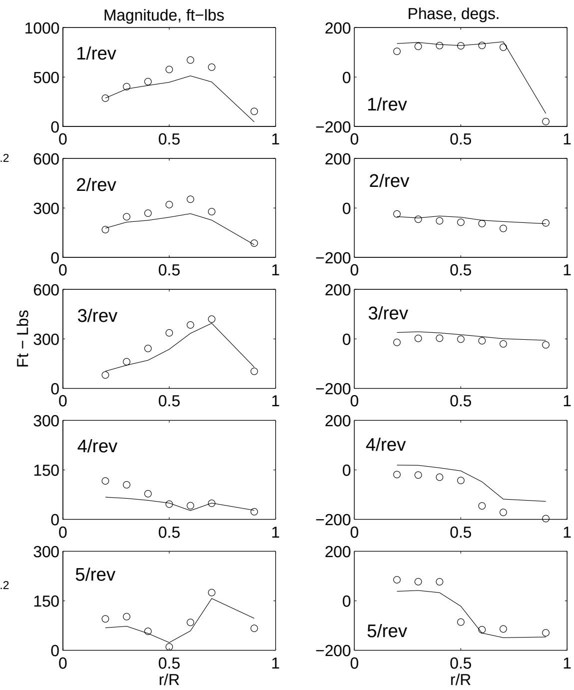

(e) Harmonic content of vibratory flap bending moment

Figure 6: **Predicted and measured flap bending moments for UH-60A Black Hawk using airloads measured in flight test; $C_W/\sigma = 0.0783$, high-speed $\mu = 0.368$**

Finally, the CFD analysis is coupled with UMARC comprehensive analysis. The method used is referred to as *loose coupling* as the transfer of information between the two analyses occurs only every rotor revolution. References [19, 20, 21, 22] have studied loose coupling schemes. In general, significant convergence problems were noted during pitching moment coupling. A *tight coupling*, though numerically expensive, is a more rigorous approach where the structural and fluid equations are integrated simultaneously at every time step. Reference [?] showed tight coupling results for the UH-60A rotor using measured trim angles. Results showed discrepancies in the high frequency components. Reference [24] shows tight coupling results for the PUMA he-

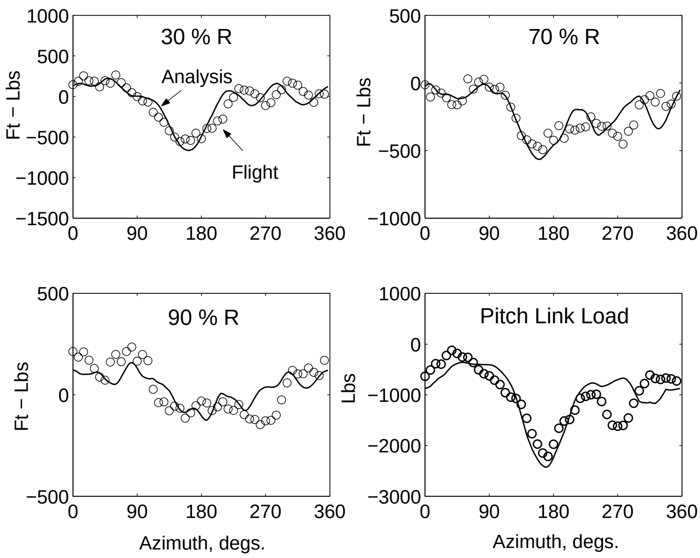

(a) Predicted and measured torsion bending moments and pitch-link load

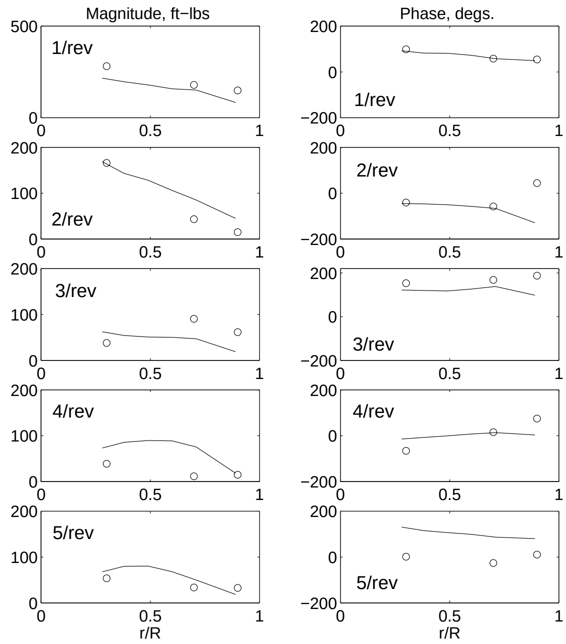

(b) Harmonic content of torsion moment

Figure 7: **Predicted and measured torsion bending moments and pitch link load for UH-60A Black Hawk using airloads measured in flight test; C_w/σ = 0.0783, high-speed μ = 0.368,**

licopter. Initial calculations for the UH-60A were unstable due to inaccurate pitching moments. Reference [25] have used tight coupling to produce good correlation of chordwise pressure data for the ONERA 7A model rotor. Reference [26] studied tight coupling, but the calculations were again performed at prescribed control angles and hence did not ensure the simultaneous convergence of trim and response equations.

In the present study both CFD generated lift and pitching moments are consistently coupled to obtain stable high-speed solutions for the UH-60A helicopter. The control angles are not assumed but calculated based on vehicle force and moment balance thereby demonstrating the simultaneous convergence of trim, response and fluid dynamics equations. Loose coupling is employed because of its non-prohibitive computational cost and as a first step for performing coupled rotor aeroelastic analysis.

PREDICTION OF BLADE DEFLECTIONS WITH MEASURED AIRLOADS

Measured lift, chord force, pitching moment, lag-damper force and rotor control angles are used to calculate the structural response of an isolated rotor. The prediction errors would originate entirely from structural modeling. The main rotor is modeled as a fully articulated beam with flap and lag hinges coincident at 4.66% span. All blades are identical. Each blade is defined by 20 finite elements undergoing flap, lag, torsion and axial degrees of motion. The blade property data, including nonlinear aerodynamic and structural twist distributions are obtained from the NASA Ames Master Database [27, 28]. The tip sweep in the outer 6.9% of the blade span (reaching a maximum of 20 degrees at 94.5% span) is modeled as structural (center of gravity) and aerodynamic (aerodynamic center) offsets from a straight undeformed elastic axis. The lag-damper force is imposed on the blade using the nominal geometry described in the Database. The torsion boundary condition consists of a rotary spring of stiffness 363 ft-lbs/ft [29]. The flap, lag and pitch stiffness and damper values of the elastomeric bearing are included as linear springs and dampers. The rotor blade frequencies are shown in Fig 3. The frequencies are calculated at the measured collective angle of 13.21 degrees.

The measured airloads are in the deformed blade frame, and contain the loading caused by the undeformed blade as well as by the aeroelastic response. They are reduced to the undeformed frame iteratively using calculated deformations at each step. The periodic blade response is calculated directly using finite element in time. A time-marching algorithm, in comparison, requires more than an order of magnitude longer in computation time to settle down to the final steady state

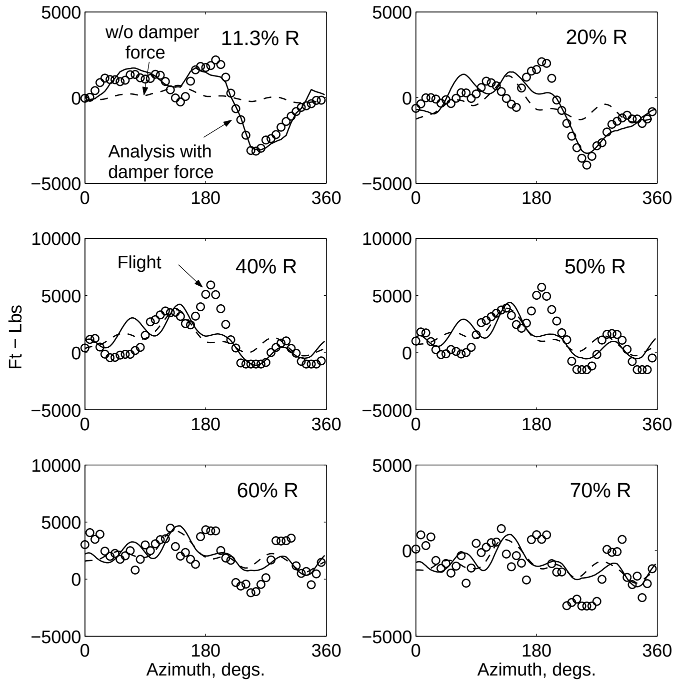

Figure 8: **Predicted and measured chord bending moments for UH-60A Black Hawk with and without measured damper force; C_W/σ = 0.0783, high-speed μ = 0.368**

response. In addition, artificial damping is required initially during convergence cycles and needs to be subsequently removed. Artificial damping accelerates the decay of the initial natural mode response in absence of aerodynamic damping.

The calculated oscillatory flap angle at the blade root is shown in Fig 4. The waveform is sensitive to structural damping in the 1st flap mode. A damping value of 4% critical is used to obtain a good peak to peak match. The phase of the resulting waveform shows satisfactory agreement. There is an under-prediction of higher harmonics at the end of the second quadrant. The calculated oscillatory lag angle at the blade root is shown in Fig 5. The phase of the calculated waveform is slightly shifted in the advancing blade. In general it shows similar trends as the test data.

The predicted flapwise bending moment distributions are compared with test data in Fig 6. The predicted steady values are within 10% of flight test values, except at the 70% radial station, and are not included for comparison. The total (1-10/rev) and vibratory components (3-10/rev) of the bending moment show similar trends as the test data. Figure 6(e) shows the radial distribution of bending moment harmonics, both magnitude and phase. The vibratory harmonics, 3-5/rev show similar qualitative trends, although the magnitudes of 3/rev and 4/rev are under-predicted at the midspan stations and inboard stations respectively.

The torsion bending moments at three radial stations and the pitch link load are shown in figure 7(a). The steady values are equated with that of the flight test data. Predictions in the retreating blade require further refinement. Predicted values show similar oscillations in the third and fourth quadrant as the test data but the phase prediction is inaccurate (30% R). The peak magnitude of these oscillations are also under-predicted. This discrepancy increases outboard (70% R and 90% R) and the integrated effect is seen on the pitch link loads. Torsional deformations in the advancing blade are crucial for accurate airloads prediction. Predicted torsion moments in the advancing blade show the correct trends. The harmonic content of the torsion moments are shown in in Fig 7(b). The large error in 3/rev prediction is the source of discrepancy in the fourth quadrant. The 4/rev shows a large error at the 70% R station. Out of all the harmonics of elastic torsion, 2-4/rev have the maximum contribution to vibratory lift (3-5/rev) through the azimuthal velocity variation. And of these three, 2/rev is the largest contributor. Prediction of 2/rev shows satisfactory trends in magnitude and phase.

The calculated chord bending moment is shown in Fig 8 both with and without the damper force. The root chord moment (11.3% R) is dominated by the non-linear lag damper force. The sharp gradient at the junction of the third and fourth quadrant is a direct effect of the lag damper. Predictions with measured damper force show good agreement with test data. The damper acts at 7.6% R and has a significant effect on the moments up to 40% R. In the mid-span stations (40% R, 50% R) the flight test data shows a sharp peak at the junction of the second and third quadrants. The predictions fail to capture this peak. Towards the outboard stations (70% R) predictions are unsatisfactory. The measured chord force contains only the induced component. The effect of viscous drag can play an important role on the chord bending moments at the outboard stations. In general, the 5/rev nature of the chord bending moments are well predicted.

In conclusion, measured airloads, control angles and damper forces are used to obtain a set of blade deformations which is close to the actual values. These deformations are now used to calculate airloads.

PREDICTION OF AIRLOADS WITH PRESCRIBED DEFLECTIONS

The deflections obtained in the previous section are now used to calculate airloads. The prediction errors would originate entirely from aerodynamic modeling. Airloads are calculated using two methods - (i) a Weissinger-L (W-L) type lifting line model and (ii) 3-D

CFD. The predictions are compared and the deficiencies of the lifting line model investigated.

LIFTING-LINE MODEL

The W-L lifting line model is used with a refined Bagai-Leishman pseudo-implicit free wake model [7], 2D airfoil tables and Leishman-Beddoes 2D unsteady model for attached flow formulation [8, 9]. The attached flow formulation is used because there is no evidence of dynamic stall at this flight condition [30]. The unsteady model is semi-empirical in nature and have been validated and refined using experimental data from symmetric airfoils - NACA 0012, Boeing-Vertol V23010-1.58 and NACA 64A010. Reference [11] showed that refining the model for the Black Hawk airfoils, SC1095 and SC1095 R8 does not improve airload predictions. Therefore in the present study the original Leishman-Beddoes model is retained.

The airloads are calculated using the following iterative procedure. In the first step, the prescribed blade deflections, measured control angles, and an uniform inflow obtained from the measured thrust are used to calculate the sectional angle of attack. The sectional angle of attack and the incident normal Mach number are used to calculate sectional lift using the airfoil tables. From the lift, the bound circulation strengths are calculated using Kutta-Joukowski theory. In the second step, the bound circulation strengths are used to calculate the rotor free wake using a single rolled up tip vortex model. With the new free wake generated inflow, the sectional angle of attack distribution is recalculated. In the third step, the new angle of attack distribution is used as input to the W-L model to recalculate the bound circulation strengths. Steps two and three are performed iteratively until the bound circulation converges. Three iterations are enough for this purpose.

Within the above general procedure the airfoil tables are included by two methods. In the first method, the angle of attack obtained in step two is scaled to an equivalent flat plate angle of attack using the lift obtained from the airfoil tables. This scaled angle of attack is used in step three. The resultant bound circulation strength is then used directly to compute lift using the K-J theorem. In the second method the angle of attack in step two is not scaled but provided directly as input to step three. Bound circulation strength obtained in step three is not used to calculate lift using K-J. Instead, they are used to calculated the circulation strengths of near wake trailers. These near wake trailers are used to estimate the induced angle of attack at quarter chord points. This induced angle of attack is subtracted from the angle of attack in step two and the resulting effective angle is used to obtain lift from the airfoil tables.

The rotor is not re-trimmed for control angles and inflow. Therefore, the steady and 1/rev components of lift are removed for comparison with flight test data. Figure 9(a) shows predicted blade lift at four radial stations. Predicted lift from the two airfoil look-up methods are almost identical. Compared to the comprehensive analysis predictions (Fig 2), significant improvement is obtained in the advancing blade. This is a reflection of improved 2/rev lift coming from accurate 1/rev elastic torsion. Prediction of vibratory lift (3-10/rev) remains unsatisfactory. The measured vibratory lift shows a characteristic up-down impulse in the advancing blade followed by a second excitation. This phenomenon is most conspicuous inboard (67.5% R and 77.5% R) and is the source of all vibratory harmonics. Towards the tip (92% R and 96.5% R) the vibratory lift shows a dominant 3/rev charater. Predictions are inaccurate both inboard and towards the tip.

The 2D test airfoil tables are now replaced with CFD generated tables, both for the SC1095 and SC1095 R8 airfoils. Figure 9(b) shows that using 2D CFD tables produces accurate prediction of vibratory lift at the two outboard stations. This is because the 2D CFD lift tables agree closely with the test airfoil tables up to Mach number 0.7. However, above Mach 0.7, there is significant deviation. Figure 9(b) suggests that the CFD lift airfoil tables may be more accurate than the test airfoil tables. The pitching moment tables are however similar for all Mach numbers.

Figure 10 shows the predicted pitching moments at four radial stations. The steady component is removed for comparison. Predictions are unsatisfactory at all radial stations. Similar to state-of-the-art comprehensive analyses the peak oscillations are over-predicted inboard (77.5% R) and under-predicted near the tip (96.5% R).

3-D CFD MODEL

The CFD computations are performed using an in-house modified version of the TURNS research code [33, 34]. TURNS uses a finite difference numerical algorithm that evaluates the inviscid fluxes using an upwind-biased flux-difference scheme [35, 36]. The van Leer monotone upstream-centered scheme for conservation laws (MUSCL) approach is used to obtain second and third order accuracy with flux limiters to be Total Variation Diminishing (TVD). The Lower-Upper-Symmetric Gauss-Seidel (LU-SGS) scheme [37] is used as the implicit operator. Though the (LU-SGS) implicit operator increases the stability and robustness of the scheme, the use of a spectral radius approximation renders the method only first order accurate in time. Therfore, a second order backwards differencing in time is used, along with Newton-type sub-iterations to restore formal second order time accuracy.

A single block mesh approach is used to make the

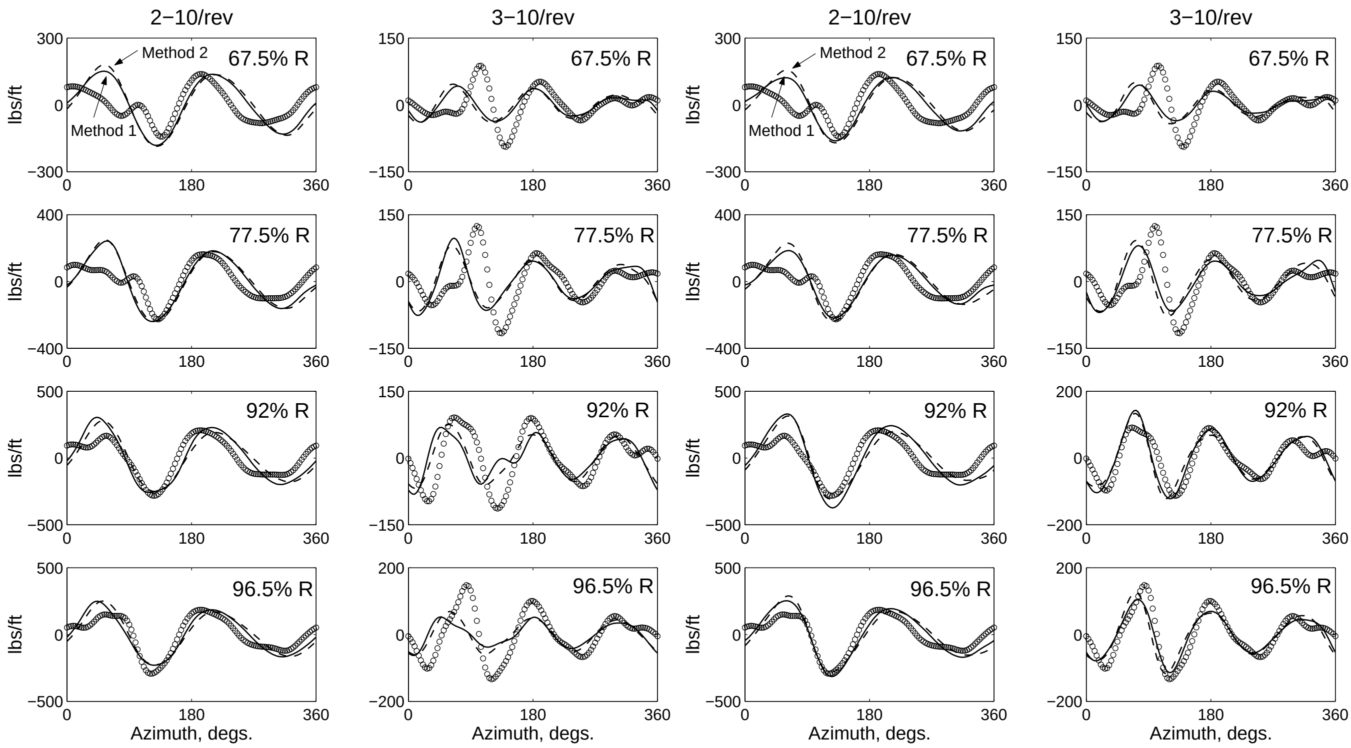

(a) Predicted lift using test airfoil tables

(b) Predicted lift using 2D CFD generated tables

Figure 9: **Prediction of lift by W-L type lifting line model using prescribed blade deformations; $\mu = 0.368$, $C_w/\sigma = 0.0783$**

calculations computationally viable. Complete wake capturing from CFD techniques requires a multiblock or overset mesh based approach. In this study only one blade of the rotor is modeled and the effects of other blades are included using an induced inflow distribution. The effects of the near shed wake, near tip vortex and bound vortices are captured fairly well in the CFD computations. Hence, only the induced inflow caused by the far-wake tip vortex need to be included to model the returning wake effects. The induced inflow is computed at each grid point using the Bagai-Leishman free wake model. The induced inflow is incorporated in to the flow solution using the *Field Velocity Approach*, which is a way of modeling unsteady flows via grid movement [38, 39].

The present numerical scheme employs a modified finite volume method for calculating the grid and time metrics. The modified finite volume formulation has the advantage that both the space and time metrics can be formed accurately and free stream is captured accurately [40]. The aeroelastic deformations are included into the flow solutions by moving the mesh points to conform to the surface geometry of the deformed blade in a consistent manner. The use of such dynamically deforming mesh geometry mandates the recomputation of space and time metrics at each time step. These quantities are computed in a manner which satisfies the *Geometric Conservation Law* (GCL) [39]. The GCL is used to satisfy the conservative relations of the surfaces and volumes of the control cells in moving meshes.

Computational Grids Used

Body conforming curvilinear meshes which follow both C-H and C-O grid topologies are constructed around the UH-60A rotor blade. The C-H grid topology approximates the tip of the blade to a bevel tip, where as the C-O mesh provides a better tip definition. The computations were performed for the same deflections sets using different grid topologies to understand the impact of tip modeling present in the airload prediction. Also, coarse and refined meshes are used to quantify grid dependence of the flow simulation. The refined meshes used 217 points in the wrap around direction of which 145 are on the airfoil surface, 71 points in the normal direction and 61 points in the spanwise direction. Representative C-H and C-O mesh topologies that emphasise the salient features are shown in Fig 11. The outer boundaries for the 3-D meshes are about 10 chords away from the blade surface. The details of grid and time independence studies are described in reference [13]. All results presented in this paper are using the refined C-H mesh with an azimuthal time step of 0.25^o.

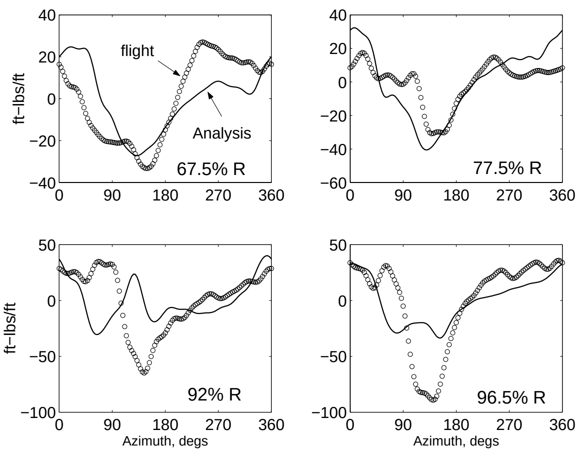

Figure 10: **Prediction of quarter-chord pitching moments by W-L type lifting line model using prescribed blade deformations; $\mu = 0.368$, $C_w/\sigma = 0.0783$**

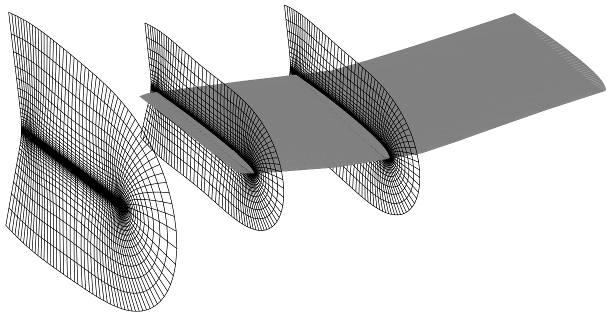

(a) C-H mesh

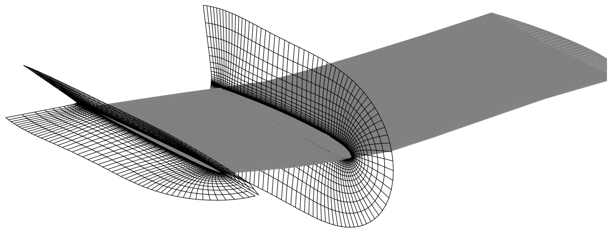

(b) C-O mesh

Figure 11: **Near body C-H and C-O meshes at the blade tip**

Deformation Scheme

The structural dynamic analysis provides deformations as functions of radius and azimuth of form $[u(r,\psi), v(r,\psi), w(r,\psi), v'(r,\psi), w'(r,\psi), \phi(r,\psi)]^T$, where u,v, w are the linear deformations in axial, lag and flap directions, v', w' are the radial derivatives for flap and lag degrees and ϕ is the elastic torsional deformation. The given rotor geometry is dynamically deformed in accordance with these blade motions. At any section one could define a rotation matrix T_{DU} which is a function of the rotation angles v', w' and ϕ. Then the deformed mesh coordinates in the blade fixed frame are given by the following equation

$$\begin{bmatrix} x' \\ y' \\ z' \end{bmatrix} = (T_{DU})^T \begin{bmatrix} x \\ y \\ z \end{bmatrix} + \vec{x_{lin}} \qquad (0.1)$$

The vector $\vec{x_{lin}}$ represents the linear deflections given by $\{u, v, w\}^T$. Once the deformed mesh is obtained in the blade fixed frame, it is rotated about the z-axis to the appropriate azimuthal location. A cosine decay is applied to both the rotations and linear deflections such that the outer boundary of the mesh remains stationary.

Predicted Airloads

The predicted normal force (2-10/rev and 3-10/rev) and pitching moments (1-10/rev) obtained using CFD are shown in Figures 12(a) and 13. Predictions show very good correlation with test data. Compared to the lifting-line model, the impulse in the advancing blade lift is accurately captured. The predicted pitching moments also show excellent correlation in both magnitude and phase with the flight test data. This leads to two important conclusions. First, the two problems of advancing blade lift phase and pitching moment prediction arise due to inaccuracies in aerodynamic modeling and not structural modeling. Second, the lift phase problem cannot be resolved only by accurate pitching moment predictions. Accurate pitching moments will produce accurate torsion. Accurate torsion alone, is not enough to produce the advancing blade impulse in the inboard stations. The CFD analysis captures the impulse because it predicts the vibratory loading accurately in the advancing blade (Fig 12(b)).

These observations suggest that the lifting-line model is unable to predict some of the 3-D unsteady compressible flow effects captured by CFD. In the next section, the CFD analysis is used to identify the aerodynamic mechanisms which lead to the good correlation. This is a pre-requisite to investigate the feasibility of applying generic corrections to improve the lifting-line model.

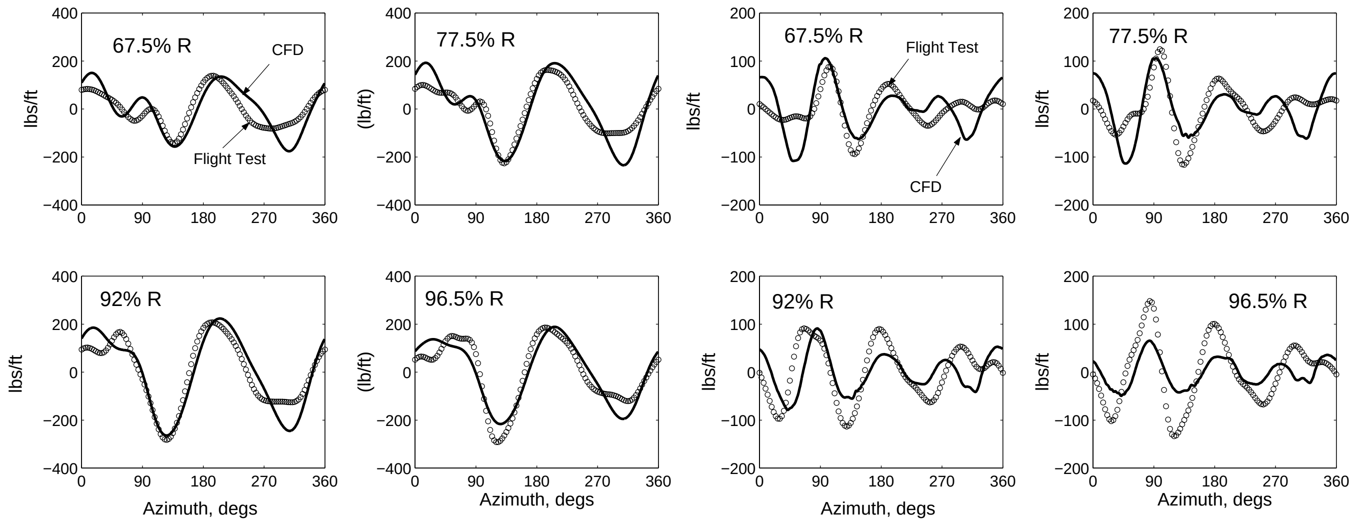

(a) Normal force (2-10/rev) predicted from CFD

(b) Normal force (3-10/rev)

Figure 12: **Predicted Normal Force using the CFD approach; $\mu = 0.368$, $C_w/\sigma = 0.0783$**

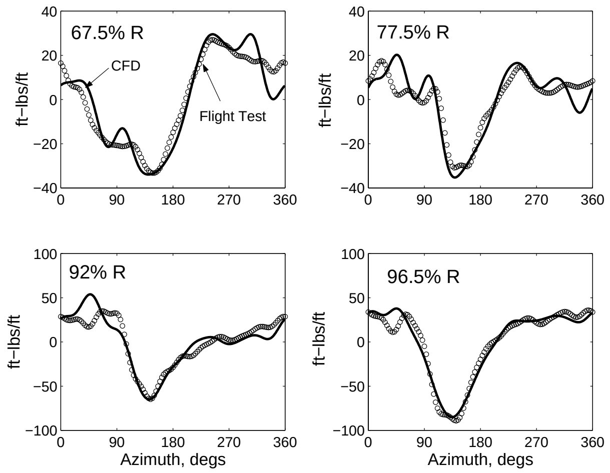

Figure 13: **Predicted Pitching Moment distributions using the CFD approach; $\mu = 0.368$, $C_w/\sigma = 0.0783$**

FUNDAMENTAL UNDERSTANDING OF AIRLOADS

In this section three fundamental mechanisms are investigated. They are: 1. Transonic effects, 2. Role of blade deformations and 3. Three dimensional effects. These are captured by the CFD accurately but are either approximated or unaccounted for by the lifting-line model.

Transonic Effects

The advancing blade lift impulse (figures 9(a) and 12(b)) is the dominant contributor to vibratory airloads over a large portion of the span (50% R to 80% R). It needs to be verified whether this phenomenon is caused by transonic effects on the advancing side. Moving shock waves are clearly visible in the surface pressure distributions (See Fig 22), although they are more predominant in the outboard regions. To isolate the transonic effects, simulations were conducted reducing the tip Mach number and maintaining the same advance ratio. The normal force obtained from these computations is shown in Fig 14(a). The normal force wave form shows the presence of the up-down impulse even at the lowest tip Mach number case. Hence, it appears that the impulsive loading in the first quadrant is not a manifestation of any transonic effects. The pitching moment waveform (Fig 14(b)) on the other hand shows significant deviation in waveform from the baseline case.

In conclusion, it is clear that transonic effects are the key contributors to the advancing blade pitching moment. However it does not have any significant effect on the impulsive loading in the advancing blade lift.

Role of Blade Motions

The role of elastic blade motions are analyzed to understand the relative influence of flap, torsion and lag degrees of freedom. This study is performed by eliminating each degree of freedom separately, one at a time, from the given set of prescribed deflections. It was observed that the elastic torsion and elastic flap degrees of freedom are the main contributors to airloads. Hence,

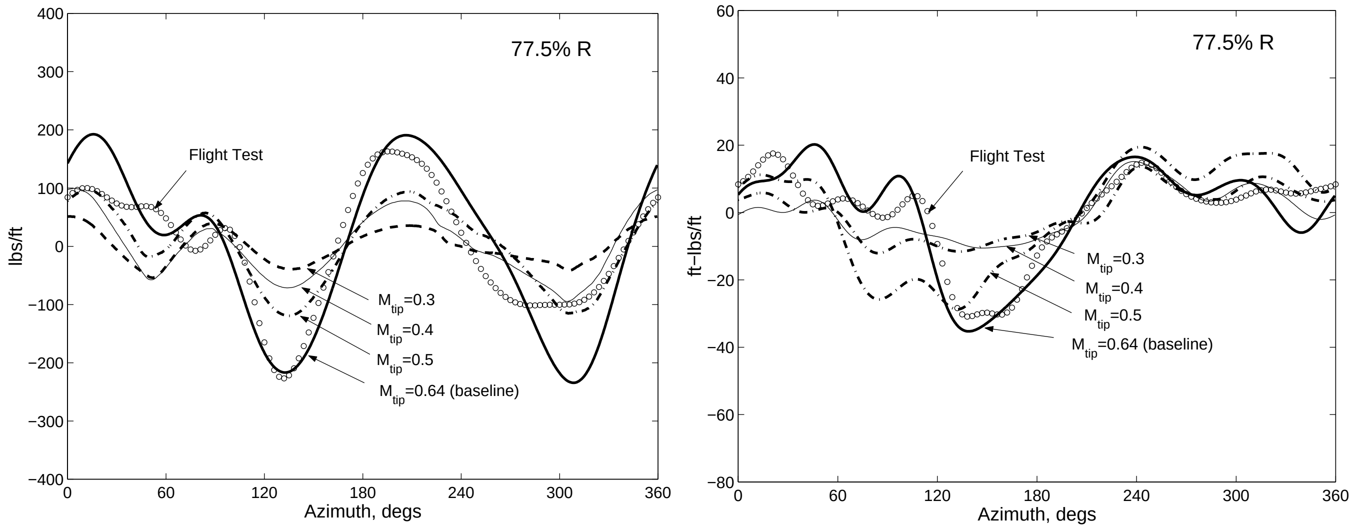

(a) Normal force (2-10/rev) predicted from CFD

(b) Pitching Moment (1-10/rev)

Figure 14: **Effects of compressibility on vibratory airloads**

the results are presented only for these two cases.

Figure 15(a) shows that the introduction of the flap degree of freedom shows the generation of the up-down impulse and a better phase correlation with the flight test data. However, there is a considerably less vibratory normal force amplitude compared to the flight test data in this case. The use of elastic torsion along with the collective and cyclic, i.e excluding the flap degree of freedom, shows improvement in the phase correlation, but shows larger amplitude. The baseline case which includes all the rigid and elastic motions shows good correlation in both phase and magnitude. Therefore, it can be inferred that the elastic deformations (both flap and torsion) are very important for accurately capturing both the phase and magnitude of the vibratory normal force. The impulsive behavior of the normal force at the inboard stations is produced by the flap degree of freedom. But, the phase and magnitude of this impulse is sensitive to elastic torsion.

Figure 15(b) shows the vibratory pitching moment excluding flap and torsion degrees of freedom, one at a time. The sharp positive-negative oscillation between the first and second quadrant is due to the large elastic torsional deformation in the advancing side. The flap degree of freedom introduces higher harmonics in the pitching moment. In conclusion, the flap deflection appears to be the key contributor to the vibratory lift impulse in the inboard stations.

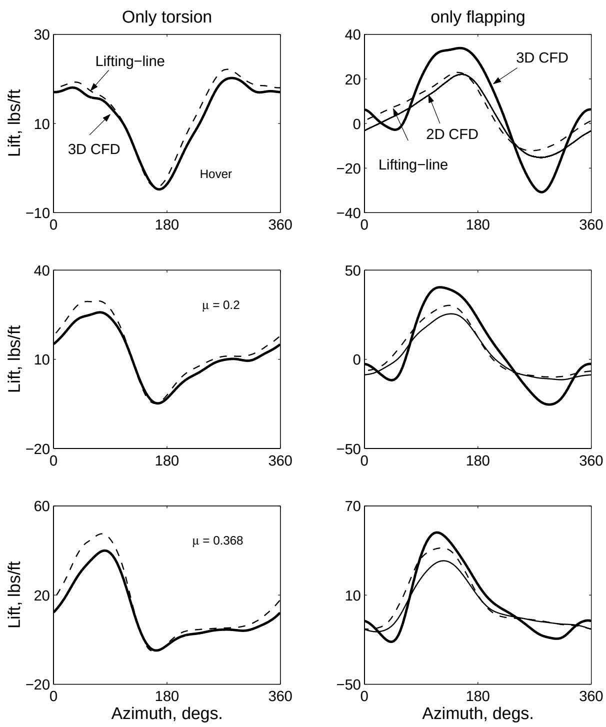

Figure 17: **Study of advancing blade lift impulse at 77.5% R; Comparing 2-D and 3-D CFD and lifting-line predictions for specific blade motions at three flight speeds**

Three Dimensional Effects

The 3-D flow effects are composed mainly of finiteness, yawed flow and spanwise curvature. The 3-D CFD calculations are now compared with 2-D CFD calculations. The 2-D CFD calculations were performed for a given section of the rotor blade by supplying the sectional

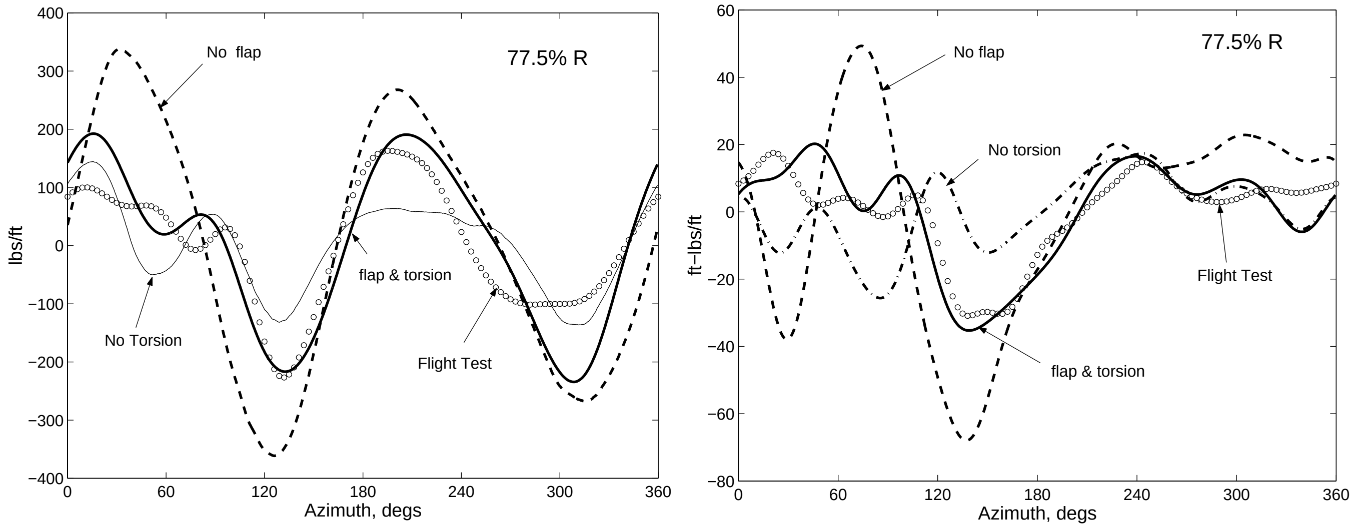

(a) Normal force (2-10/rev) predicted from CFD

(b) Pitching Moment (1-10/rev)

Figure 15: **Effects of flap and torsional degrees of freedom on vibratory airloads**

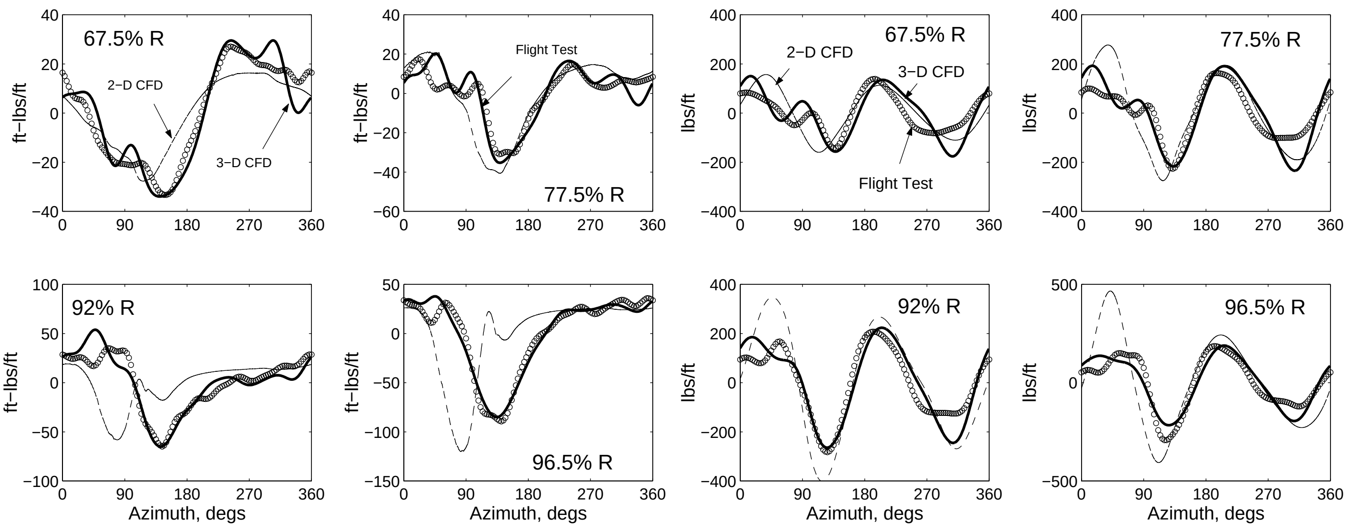

(a) Pitching Moment (1-10/rev)

(b) Normal force (2-10/rev) predicted from CFD

Figure 16: **Effects of three dimensionality in vibratory airloads**

deformations, inflow and the time varying chordwise velocity component. This can be considered as a 2-D stripwise CFD calculation. The 3-D effects are absent as the simulation is strictly 2-D with only the chordwise component of the velocity prescribed.

Figure 16(b) compares predicted normal force using 2-D and 3-D CFD computations. The 2-D CFD results are similar to the lifting-line results with the impulsive behavior missing in the advancing blade. In the previous section the impulse was identified with the flapping motion. It can now be concluded that it is a 3-D effect associated with the flapping motion. 2-D CFD predictions show larger peak to peak magnitudes compared to 3-D CFD predictions towards the tip. This is a consequence of the finiteness effects. This effect is accounted for in the lifting-line model.

Figure 16(a) compares predicted pitching moments using 2-D and 3-D CFD computations. The 2-D calculations over-predict the peak to peak moments at 77.5% R. This is again similar to the predictions obtained from the lifting line model. Therefore the phenomenon of over-prediction of inboard pitching moments is related to 3-D effects. In addition, like the normal force waveform, the 3-D pitching moments also show an impulsive behavior in the advancing blade. Towards the tip, the 2-D pitching moments shows large initial negative peak in the advancing side which is also present in the lifting line case. Further investigation revealed that the 3-D shock relief effects at the tip alleviate the initial large negative pitching moment peak. The excursion of the aerodynamic center towards the trailing edge, when the airfoil is generating positive lift is the reason for the large negative pitching moment. The shock relief effects limit this excursion of the aerodynamic center and hence alleviate the large negative pitching moments.

To investigate the limitations of the lifting-line model to capture the 3-D effect associated with flapping motion, the problem is further dissected. Starting from hover, for a progressively increasing set of forward speeds the prescribed flap and torsion deflections are used separately. Predictions are compared between 3-D CFD, lifting-line and 2-D CFD models. Figure 17 shows that for the torsion deflection both lifting-line and 3-D CFD predict similar lift. Significant discrepancy is noted for the flap deflection. This discrepancy is independent of forward speed and is therefore not a purely high-speed phenomenon. The 2-D CFD results agree well with the lifting-line predictions suggesting that the discrepancy is not a 2-D nonlinear effect but a purely 3-D phenomenon.

SPANWISE CURVATURE

The flap bending curvature (w'') is observed to contribute to the advancing blade lift impulse. The bending curvature changes rapidly at the inboard stations in the advancing blade. This is because the blade flap response transitions from being dominated by the 1st flap mode to being dominated by the 2nd flap mode. The 2nd flap mode has a nodal point at 78.5% R and has the largest change in slope in this region. CFD computations were performed removing the contribution of the 2nd flap mode from the flap response.

Figure 18(a) shows the normal force predictions with and without the effects of 2nd flap mode. Without the effects of curvature induced by the 2nd flap mode, 3-D CFD predictions are close to those predicted by the lifting-line model (i.e. the advancing blade impulse is absent). Therefore, it is clear further that the the three dimensional effects of the 2nd flap mode (curvature induced effects) are the primary contributors to the advancing blade lift impulse.

The pitching moments show similar trends (Figure 18(b)) in the inboard station. The impulsive character of the pitching moment is found absent when using the flap response without the 2nd flap mode contributions. However, towards the tip, there is little variation between the baseline and present case. This is true for the normal force variation also. Therefore, as expected, the curvature effects are more prominent at the inboard stations rather than at the tip.

The spanwise curvature is accounted for in the lifting-line model as the angle of attack distribution is determined relative to the deformed section. Therefore the exact aerodynamic mechanism that relates the changes in spanwise curvature to the impulsive aerodynamic loading is not clear at present. This issue is currently being investigated in detail.

CFD COUPLING WITH UMARC

As mentioned earlier, the prediction of airloads using the prescribed deflections and measured control angles shows errors in the steady and 1/rev harmonics. These errors were caused by inconsistencies in rotor trim. In this section a first principle based analysis is described to obtain a consistent blade response, trim and airload solution. The 3-D CFD model is coupled with the UMARC structural analysis using a loose coupling method.

During the initial stages of the development of the coupling procedure, it was observed that the blade response diverged abruptly after showing monotonic convergence trends. This problem was traced to large 1/rev hinge moment imbalance caused by the rotor being slightly out of trim. In trimmed forward flight the 1/rev aerodynamic normal forces reverse sign as one moves radially outboard. This is because the 1/rev airloads need to be in approximate moment balance about the hub for low steady shaft moment. Therefore, in real flight the integrated 1/rev hinge moments are relatively small. In the analysis, small variations in aerodynamic loads during the trim procedure produces large 1/rev hinge moments. In the absence of aerodynamic damping these 1/rev hinge moments diverges the flap response.

The problem was rectified by using an additional loop which adjusts the control angles iteratively to produce the same hinge moment magnitude as that produced by the first comprehensive analysis solution. This step uses the lifting line model. The lifting line analysis was found to generate similar 1/rev normal force prediction as the CFD computations. Response convergence was obtained after the introduction of this additional correction. It is to be noted that all lift, drag and pitching moment obtained from the CFD computations are coupled to structural analysis in this approach. Earlier loose coupling efforts have shown divergence of torsional response. This is evidently because of the discrepency in the pitching moment predictions.

Briefly, the algorithm is as follows.

1. *Obtain an initial guess for control angles and structural response using UMARC comprehensive anal-*

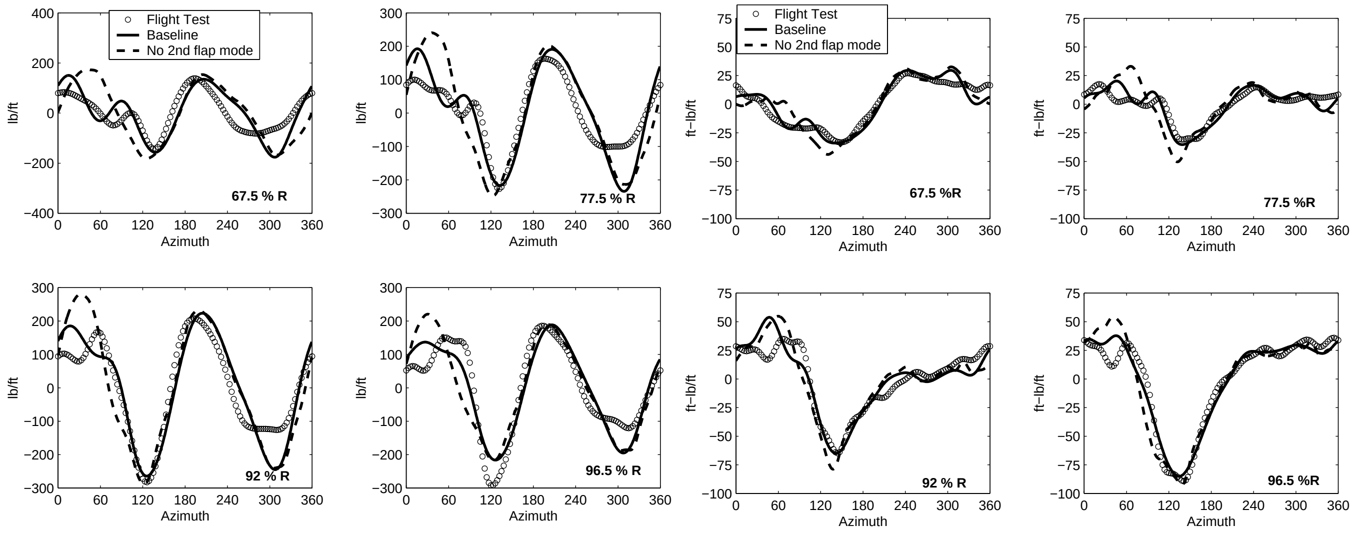

(a) Normal force (2-10/rev) predicted from CFD

(b) Pitching Moment (1-10/rev)

Figure 18: **Effects of the 2nd flap mode on the vibratory airloads**

ysis solution. The sensitivity of the control angles to the vehicle trim residues (trim jacobian) is evaluated.

2. *Use the lifting line model to iteratively add corrections to the control angles (aeroelastic deformations are unchanged) to produce the same hinge moment amplitude as that obtained in step 1.*

3. *Calculate CFD airloads using the above control angles and the prescribed blade motions.*

4. *Calculate structural deformations using the CFD airloads (normal force, pitching moment and chord force) as the forcing function.*

5. *Correct the control angles according to the rotor trim residues.*

6. *Check for blade response and trim convergence. If the convergence condition is not satisfied return to step 2.*

The coupling procedure converged to the prescribed numerical limit within 8 iterations. The convergence history of the blade response at the tip (flap and torsion) is shown in Fig 19. The total normal force and pitching moment (all harmonics) at each coupling iteration are shown in Fig 20. It can be observed that the changes in control angles change the steady and 1/rev harmonic, while the higher harmonics are relatively unaffected. The final converged normal force shows improved normal force phase compared to the baseline comprehensive analysis (Fig 2). The pitching moments show very good peak to peak magnitudes and phase correlation with the test data. The surface pressure distributions obtained at the final iteration are correlated against the available flight test data in Fig 22. The shock locations in the advancing side of the blade at the outboard radial station are predicted accurately.

Figure 21 shows the vibratory normal force (3-10/rev) at each coupling iteration. It is evident that there is little variation in the higher harmonic content with changes in control angles. Hence, it appears that one would be able to obtain good estimates of vibratory hub loads even with just one coupling iteration.

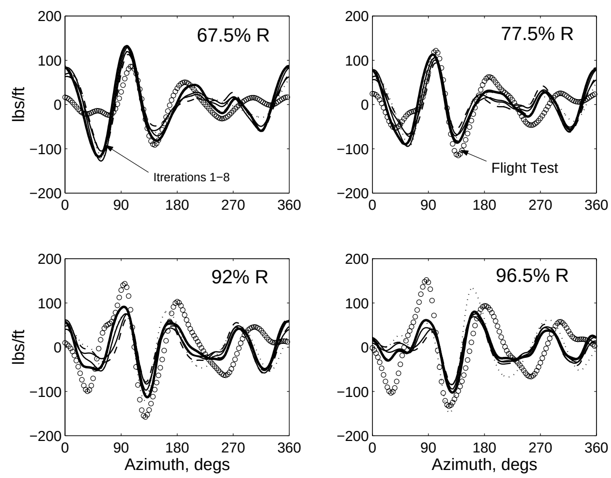

Figure 21: **Vibratory normal force (3-10/rev) variation with coupling iterations**

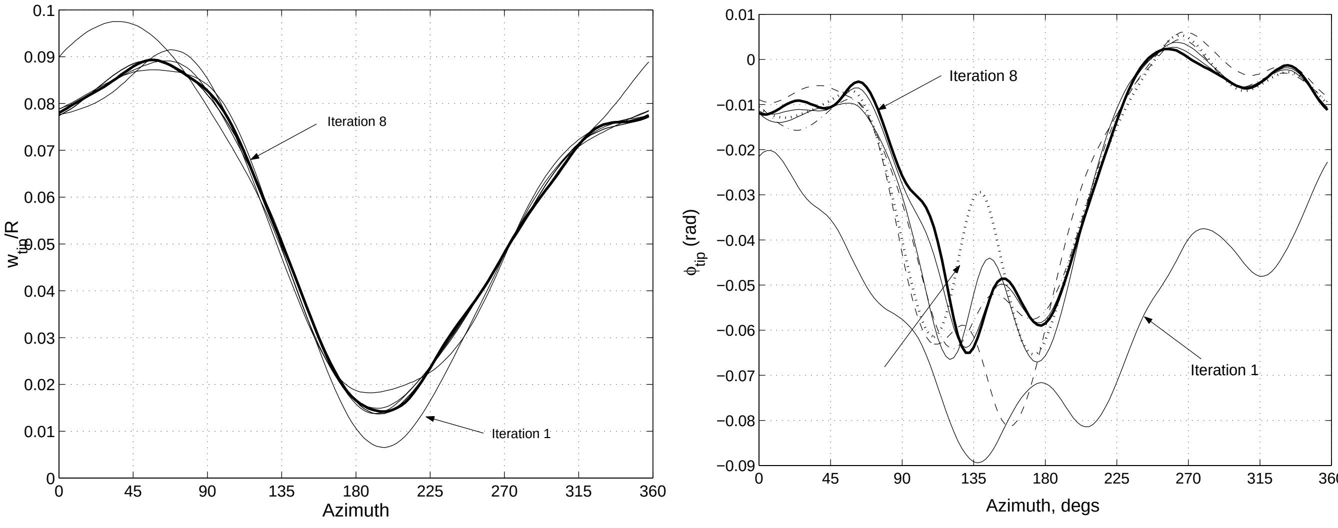

(a) Flap response at the blade tip

(b) Torsional response at the blade tip

Figure 19: **Convergence of tip elastic deformations with coupling iterations**

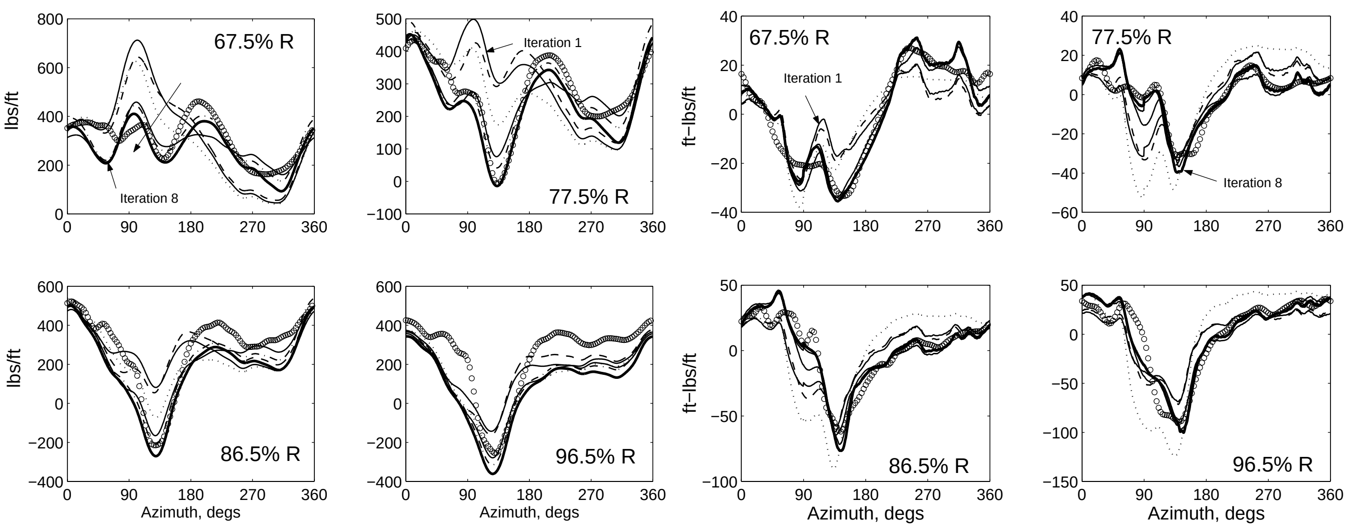

(a) Normal Force (All harmonics)

(b) Pitching Moment (1/rev and higher)

Figure 20: **Convergence of aerodynamic loads with coupling iterations**

CONCLUSIONS

Measured airloads, damper loads and control angles of the UH-60A Black Hawk in high-speed flight are used to validate the structural model of an isolated rotor. On satisfactory prediction of blade loads, the predicted blade deformations are used to calculate airloads. The airflow model is refined from a table look up based unsteady lifting-line model to a 3-D CFD model. The 3-D CFD model predicts more accurate airloads compared to the lifting-line model with the same deformations and same far wake. The CFD model is investigated to understand the limitations of the lifting-line model and identify the possible sources of improvement. Finally the CFD model is loosely coupled with the comprehensive analysis UMARC to obtain a consistent blade response, trim and airload solution from first principles.

1. Error in the prediction of advancing blade lift in high-speed flight stems from 3-D aerodynamic effects not structural modeling. Even when correct blade

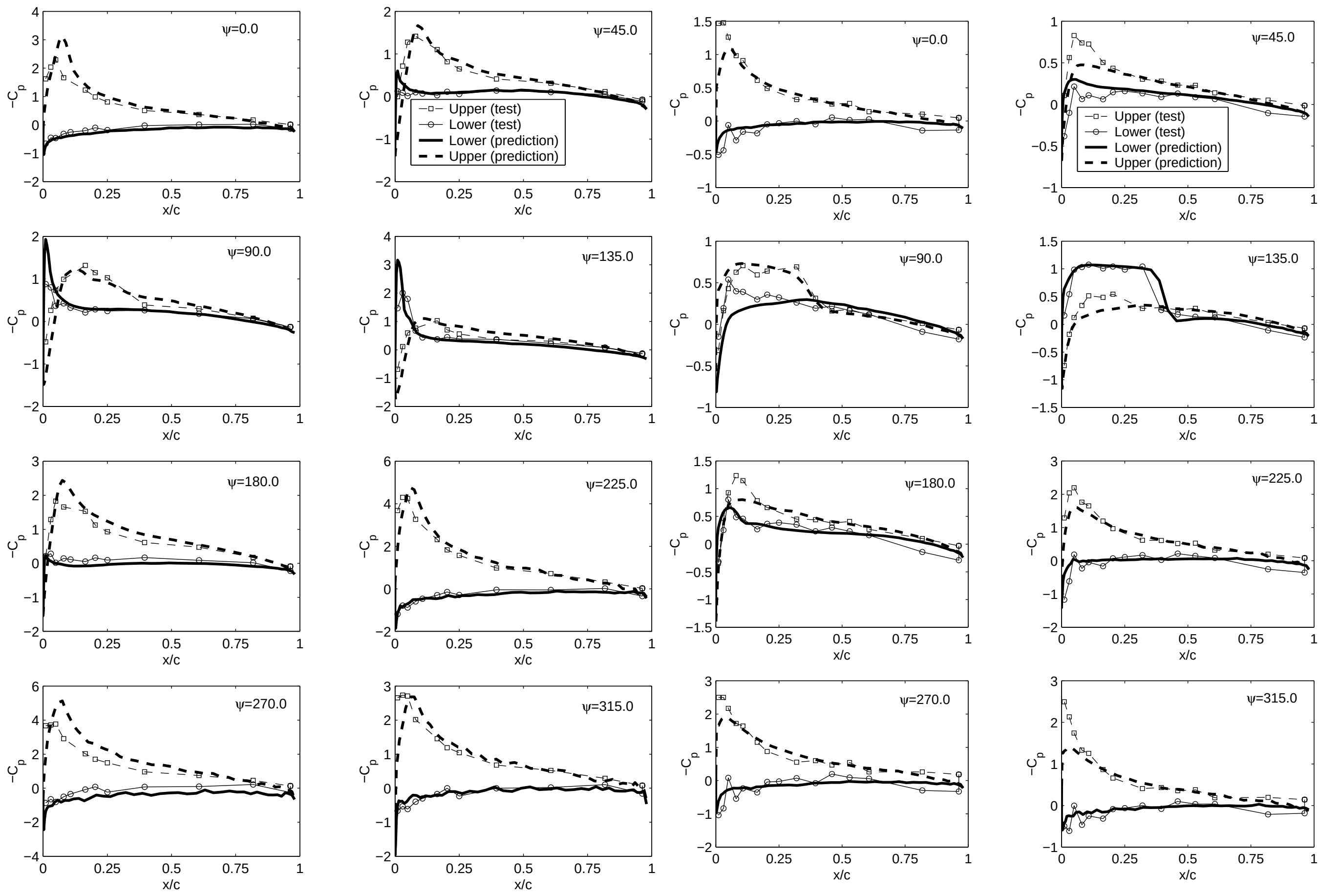

(a) 77.5%R

(b) 96.5%R

Figure 22: **Chordwise surface pressure variation with azimuth at two radial stations; μ = 0.368, C_w/σ = 0.0783**

deformations are known, a table look up based unsteady lifting-line model fails to accurately capture the advancing blade lift. A 3-D CFD model captures the lift phase accurately.

2. The advancing blade lift is dominated by vibratory harmonics (3-10/rev), except near the tip (outboard of 90%R). A Lifting-line model using CFD generated 2-D airfoil tables predict the vibratory harmonics near the blade tip (outboard of 90% R) accurately. However predictions are inacurate inboard (67.5% R, 77.5% R). Inboard, the measured vibratory harmonics exhibit an impulsive behavior in the advancing blade. The 3-D CFD model accurately picks up this impulse and therefore predicts the lift phase correctly.

3. The 3-D CFD captured advancing blade impulse in lift is not a transonic effect. This impulse is generated by 3-D aerodynamics associated with blade flapping motion. The flap bending curvature appears to play a key role.

4. Compared to comprehensive analysis, lift predicted at the inboard stations using a lifting-line model show improved correlation with test data with prescribed blade deformations. This is because of improved 2/rev lift stemming from accurate 1/rev elastic torsion.

5. The pitching moment predictions from the lifting-line model is poor. The moments are over-predicted inboard (77.5% R) and under-predicted near the tip (96.5% R). The 3-D CFD model shows accurate predictions both inboard and near the tip. This is because of the highly accurate surface pressure predictions obtained using CFD.

6. Near the tip, it is the 3-D transonic effects (shock relief) that play the key role in determining the peak to peak magnitude and phase of pitching moment.

At the intermediate span stations 60% to 80% the three dimensional effects associated with flap bending contribute to the phase and magnitude of the pitching moments.

7. Consistent coupling of 3-D CFD generated lift, chord force and pitching moments with UMARC structural analysis improves airloads prediction compared to state-of-the-art comprehensive analysis. Eight iterations are required to obtain a coupled aeroelastic solution. The resultant vibratory airloads appear insensitive to small changes in rotor trim angles. Therefore for design purposes only one or two iterations of CFD calculations may be sufficient.

ACKNOWLEDGEMENTS

The authors acknowledge the active participation of Beatrice Roget. The authors gratefuly acknowledge the support provided by the National Rotorcraft Technology Center with Dr. Yung Yu as technical monitor. The authors thank Jim Duh, Charles Berezin (Sikorsky Aircraft Corp.), William Bousman, Robert Ormiston and Hyeonsoo Yeo (Army/NASA) for providing input data, flight test data and for their valuable comments and advice.

REFERENCES

[1] Hansford, R. E. and Vorwald J., “Dynamics Workshop On Rotor Vibratory Loads”, 52nd Annual Forum of the AHS, Washington D.C., June 4-6 1996.

[2] Bousman, G., “The Response of Helicopter Rotors to Vibratory Airloads”, American Helicopter Society National Specialists’ Meeting on Rotorcraft Dynamics, Arlington, Tex., Nov 13-14, 1989.

[3] Hooper, R. E., “The Vibratory Airloading of Helicopter Rotors”, 9th European Rotorcraft Forum, Sep 13-15, Stesa, Italy, 1983

[4] Bousman, G., and Kufeld, R. M., Balough, D., Cross, J. L., Studebaker, K. F., Jennison, C. D., “Flight Testing the UH-60A Airloads Aircraft”, 50th Annual Forum of the American Helicopter Society, Washington, D.C., May, 1994.

[5] Bousman, G., “Putting the Aero back into Aeroelasticity”, 8th Annual ARO Workshop on Aeroelasticity of Rotorcraft Systems, Pennsylvania State University, University Park, PA, October 18-20, 1999.

[6] Ganguli, R. and Chopra, I., “Aeroelastic Optimization of an Advanced Geometry Helicopter Rotor”, Proceedings of the 33rd AIAA Structures, Structural Dynamics and Materials Conference, Dallas, Texas, April 1992.

[7] Bagai, A. and Leishman, J. G., “The Maryland Free-Wake Analysis - Theory, Implementation and User’s Manual,” University of Maryland, Department of Aerospace Engineering, Technical Report Prepared for NASA Langley Research Center, Aeroacousitics Branch, Fluid Mechanics and Acoustics Division, Contract No. 015-2685, December 1995.

[8] Leishman, G. J., “Validation of Approximate Indicial Aerodynamic Functions for Two-Dimensional Subsonic Flow”, *Journal of Aircraft*, Vol. 25, No. 1, October 1, 1988.

[9] Beddoes, T. S., “Practical Computation of Unsteady Lift”, Proceedings of the 7th European Rotorcraft Forum, Sept. 1982, see also *Vertica*, Vol. 8, No. 1, 1984, pp. 55-71.

[10] Datta, A. and Chopra, I., “Validation and Understanding of UH-60A Vibratory Loads in Steady Level Flight”, 58th Annual Forum of the American Helicopter Society, Montreal, Canada, June 2001.

[11] Datta, A. and Chopra, I., “Validation of Structural and Aerodynamic Modeling using UH-60A Flight Test Data”, 59th Annual Forum of the American Helicopter Society, Phoenix, Arizona, May 6-8, 2003.

[12] Lim, J. W. and Anastassiades, T., “Correlation of 2GCHAS Analysis with Experimental Data”, *Journal of the American Helicopter Society*, Vol.40, No. 4, October 1995, pp. 18-33.

[13] Sitaraman, J., Baeder, J. D., and Chopra, I., “Validation of UH-60 Rotor Blade Aerodynamic Characteristics using CFD,” , 59th Annual Forum of the American Helicopter Society, Phoenix, Arizona, May 6-8, 2003.

[14] Esculier, J. and Bousman, G., “Calculated and Measured Blade Structural Response on a Full-Scale Rotor”,*Journal of the American Helicopter Society*, Vol.33, No.1, January 1988, pp. 3-16.

[15] Hodges, D. H., and Dowell, E. H., “Nonlinear Equations of Motion for the Elastic Bending and Torsion of Twisted Nonuniform Rotor Blades”, NASA TN D-7818.

[16] Ormiston, R. A., Hodges, D. H., and Peters, D. A., “On the Nonlinear Deformation Geometry of Euler-Bernoulli Beams,” NASA Technical Paper 1566.

[17] Torok, M. S., Goodman and Kufeld, R., “Analysis of Rotor Blade Dynamics using Experimental UH-60A airloads obtained at the DNW,” *Journal of the American Helicopter Society*, Vol. 39, No. 1, 1994, pp. 63-69.

[18] Torok, M.S. and Berezin, C., "Aerodynamic and Wake Methodology Evaluation Using Model UH-60A Experimental Data," *Journal of the American Helicopter Society*, Vol. 39, No. 2, 1994, pp. 21-29.

[19] Tung, C., Caradonna, F., X. and Johnson, W., "The Prediction of Transonic Flows on an Advancing Rotor," *Journal of American Helicopter Society*, Vol. 32, No. 7, 1986, pp. 4-9.

[20] Strawn, R.C., Desopper, A., Miller, J. and Jones, A., "Correlation of Puma Airloads - Evaluation of CFD Prediction Methods," Paper No. 14, 15th European Rotorcraft Forum, Sept 1989.

[21] Yamauchi, G.K., Heffernan, R.M., and Gaubert, M., "Correlation of SA349/2 Helicopter Flight Test Data with a Comprehensive Rotorcraft Model," *Journal of American Helicopter Society*, Vol. 33, No. 2, 1988, pp. 31-42.

[22] Kim, K. C., Desopper, A. and Chopra, I., "Blade Response Calculations Using Three-Dimensional Aerodynamic Modeling," *Journal of American Helicopter Society*, Vol .36, No. 1, 1991, pp. 68-77.

[23] Bauchau, O.A. and Ahmad, J.U., " Advanced CFD and CSD Methods for Multidisciplinary Applications of Rotorcraft Problems," AIAA 6th Symposium on Multidisciplinary Analysis and Optimization, Seattle, WA, Sept. 1996.

[24] Rutkowski, M., J., Ruzicka, G., C., Ormiston, R., A., Saberi, H., Yoon, J., "Comprehensive Aeromechanics Analysis of Complex Rotorcraft Using 2GCHAS," Journal of the American Helicopter Society, Vol. 40, No. 4, October, 1995, pp 3-15.

[25] Buchtala, B., Wehr, D. and Wagner, S., "Coupling of Aerodynamic and Dynamic Methods for Calculation of Helicopter Rotors in Forward Flight," Proceedings of 23rd European Rotorcraft Forum, pp. 5.1-5.12, Dresden, Germany, September 1997.

[26] Pomin, H. and Wagner, S. "Navier-Stokes Analysis of Helicopter Rotor Aerodynamics in Hover and Forward Flight," AIAA 2001-0998, Reno, NV Jan 2001.

[27] Bousman, G., "UH-60A Airloads Program Data", NRTC/RITA Rotorcraft(RC) Airload Workshop, 28 Aug. 2001, The Boeing Company, Philadelphia, PA.

[28] Yeo, H., "Comprehensive Analysis of the UH-60A", NRTC/RITA Rotorcraft(RC) Airload Workshop, 28 Aug. 2001, The Boeing Company, Philadelphia, PA.

[29] Kufeld, R.M and Johnson, W., "The Effects of Control System Stiffness Models on the Dynamic Stall Behavior of a Helicopter", 54th Annual Forum of the American Helicopter Society, Washington, D.C., May 20-22, 1998.

[30] Coleman, C. P. and Bousman, G., "Aerodynamic Limitations of the UH-60A Rotor", American Helicopter Society Aeromechanics Specialists Conference, San Francisco, CA, January 19-21, 1994.

[31] Lomax, H., Heaslet, M.A., Fuller, F.B., and Sluder, L., "Two and Three Dimensional Unsteady Lift Problems in High Speed Flight", NACA Rept. 1077, 1952.

[32] Ballhaus, W. F. and Goorjan, P. M., "Computation of Unsteady Transonic Flows by the Indicial Method", *AIAA Journal*, Vol. 15, No.2, Feb. 1978, pp. 117-124.

[33] Srinivasan, G.R. and Baeder, J.D., "TURNS: A Free Wake Euler/ Navier-Stokes Numerical Method for Helicopter Rotors," *AIAA Journal*, Vol. 31 No. 5, 1993, pp. 959-962.

[34] Srinivasan, G. R., Baeder, J., D., Obayashi, S., McCroskey, W., J., "Flowfield of a Lifting Rotor in Hover: A Navier-Stokes Simulation," *AIAA Journal*, Vol.30, No. 10, 1992.

[35] Roe, P. L., "Approximate Riemann Solvers, Parametric Vectors, and Difference Schemes," *Journal of Computational Physics*, Vol. 43, No. 3, 1981, pp. 357-372.

[36] Vatsa, V. N., Thomas, J. L., and Wedan, B. W., "Navier-Stokes Computations of Prolate Spheroids at Angle of Attack," AIAA Paper 87-2627, Aug. 1987.

[37] Jameson, A. and Yoon, S., "Lower-Upper Implicit Schemes with Multiple Grids for the Euler Equations," *AIAA Journal*, Vol. 25, No. 7, 1987, pp. 929-935.

[38] Paramesvaran, V. and Baeder, J. D., "Indicial Aerodynamics in Compressible Flow - Direct Computational Fluid Dynamic Calculations," *Journal of Aircraft*, Vol. 34, No. 1, 1997, pp. 131-133.

[39] Sitaraman, J., Baeder, J. D. and Iyengar, V., "On the Field Velocity Approach and Geometric Conservation Law for Unsteady Flow Simulations, AIAA paper 2003-3835, Orlando, Florida.

[40] Vinokur, M., "An Analysis of Finite-Difference and Finite-Volume Formulations for Conservation Laws," *Journal of Computational Physics*, Vol.81, No.2, March 1989, pp. 1-52.